On-line Parameter Identification of IPM Motor Using Instantaneous Reactive Power for Robust Maximum Torque Per Ampere Control

Toshihiko Noguchi

Department of Electrical and Electronics Engineering
Graduate School of Engineering, Shizuoka University
3-5-1 Johoku, Naka-ku, Hamamatsu, Shizuoka 432-8561,
Japan
ttnogut@ipc.shizuoka.ac.jp

Yuki Kumakiri

Department of Electrical and Electronics Engineering,
Graduate School of Engineering, Shizuoka University
3-5-1 Johoku, Naka-ku, Hamamatsu, Shizuoka 432-8561,
Japan
f0330108@ipc.shizuoka.ac.jp

Abstract—**The reluctance torque of an IPM motor can be effectively utilized by applying the maximum torque per ampere (MTPA) control algorithm, which improves the efficiency and the power density of the motor. However, the motor is unable to operate accurately on the MTPA curve due to the parameter mismatch caused by magnetic saturation and/or temperature variation. This paper proposes the d-axis inductance, the q-axis inductance, and the magnetic flux linkage identification strategy by using the instantaneous reactive power of the IPM motor. The key feature of the technique is robustness against the winding resistance variation. Several experimental tests have been conducted to verify the feasibility of the proposed technique, and it has been confirmed that every parameter identification can be achieved within 5 % error.**

Keywords—maximum torque control, magnetic saturation, parameter identification, instantaneous reactive power

I. INTRODUCTION

An interior permanent magnet synchronous motor (IPMSM) has several advantageous points such as high efficiency and high power density. In recent years, in order to utilize these features, the range of the applications expands to industrial, home appliance, automotive sectors and more. Moreover, from the view point of the improvement of the control performance, vector control is generally applied to obtain high response of the motor torque. Particularly, it is strongly desired to obtain the quick torque response for the traction control of the hybrid vehicles and the electric vehicles [1]-[3]. Under the vector control, the IPMSM can deliver the reluctance torque as well as the magnet torque by optimizing the motor current phase. Therefore, the maximum torque per ampere (MTPA) control which can deliver the torque with the minimum current norm is applied to the IPMSM drive. Due to the decrease of the inductance and/or the variation of the magnetic flux linkage; however, the operating point deviates from the optimal value[4]-[7]. As a result, enlargement of the copper loss occurs, resulting in the deterioration of the efficiency; hence, it is necessary to correct the operating point according to the operating condition on the basis of the on-line parameter identification of the motor.

This paper proposes an on-line parameter identification strategy of the inductances and the magnetic flux linkage of the IPMSM. The output torque characteristic is improved by the modified MTPA curve using the identified parameters. The identification must be performed with robustness to the other parameters such as a winding resistance. The algorithm, which can identify the motor parameters individually, is based on the separate frequency component injection technique. The algorithm does not have parameter sensitivity to the armature resistance. In the following sections, the variation of the MTPA curve caused by the magnetic saturation is examined, and the several experimental test results, i.e, the on-line identification of the parameters, the output torque characteristic and the parameter sensitivity are presented.

II. IMPACT OF MAGNETIC SATURATION

A relational expression of the d-axis current i_d and the q-axis current i_q which maximizes the torque per unit current can be given by

$$i_d = \frac{\psi_f}{2(L_q - L_d)} - \sqrt{\frac{\psi_f^2}{4(L_q - L_d)^2} + i_q^2} \; . \tag{1}$$
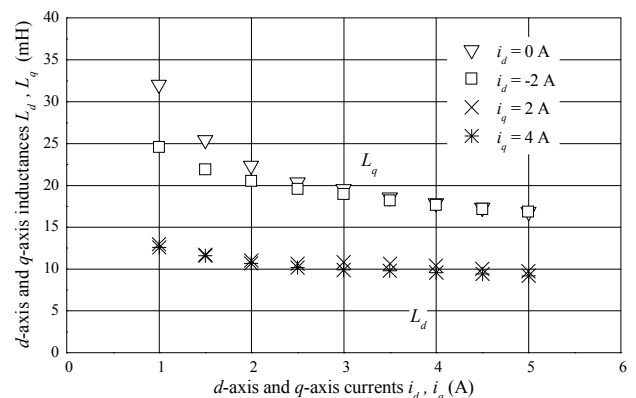
Fig. 1. Magnetic saturation characteristics.

The torque can be efficiently delivered by controlling the currents to satisfy this equation. If the parameters in (1) are varied by the magnetic saturation, the actual operating point turns away the optimum operating condition. As a result, the copper loss increases as the current amplitude increases; thus, the loss increase degrades the efficiency characteristic.

Figure 1 shows the magnetic saturation characteristics of the test motor. Although the effect of the cross saturation can be slightly seen, the d-axis inductance and the q-axis inductance monotonically decrease as the corresponding currents increase, respectively. The q-axis inductance decreases by 30~35 %, and the d-axis inductance decreases by 10 % from their nominal values. This paper discusses a robust identification strategy of these parameters.

III. VARIATION OF MTPA CURVE

Table I shows the rated values and the nominal parameters of the test IPM motor. The experimental system has been set up as shown in Fig. 2. The test motor is directly coupled with the AC servo motor (load machine) through the torque sensor. A DSP (TMS320C6713, TI) gives the gate signals to the inverter, and controls the test motor. The AC servo motor is controlled in the speed control mode, whereas the inverter controls the output torque of the test motor. The common vector control is carried out by using the rotor position which is detected by the rotary encoder. The inverter carrier frequency is 10 kHz, and the dead time is 4 μs.

The measurement of the output torque has been conducted to search the true MTPA curve. The possible combination of the d-axis current and the q-axis current has been checked out according to the following equations:

$$i_d = -I_a \sin\beta \quad, \text{ and } i_q = I_a \cos\beta . \tag{2}$$

Figure 3 shows the result of the above output torque test. The output torque has been measured at 1000 r/min. The current is controlled as expressed in (2) where the current amplitude I_a is maintained constantly and the current phase β is advanced. In Fig. 3, the plots are the measured values, and the solid lines are the torque curves calculated by (3) using the nominal values.

$$T = p\{\psi_f I_a \cos\beta + \frac{1}{2}(L_d - L_q)I_a^2 \sin 2\beta\} . \tag{3}$$

Here, p is the pole pair number. Figure 4 shows the MTPA curves. The d-axis current and the q-axis current given by (2) that maximize the output torque are plotted. The solid line is the MTPA curve given by Eq. (1) when the nominal values are used for calculation.

According to Fig. 3, significant errors between the measured values and the calculated values are observed. The errors expand as the current norm increases due to the magnetic saturation.

In Fig. 4, the true optimum operating points do not coincide with the MTPA curves calculated by (1) with the nominal values. Although the deviation is not very remarkable when the mismatch of the inductance is small, the

TABLE I.   RATED VALUES AND NOMINAL PARAMETERS OF TEST MOTOR

Number of poles	8
Rated power (W)	1000
Rated speed (r/min)	2000
Rated current (A)	3.70
Armature resistance (Ω)	1.10
Number of magnetic flux linkage (Wb)	0.174
d-axis inductance (mH)	11.0
q-axis inductance (mH)	25.0
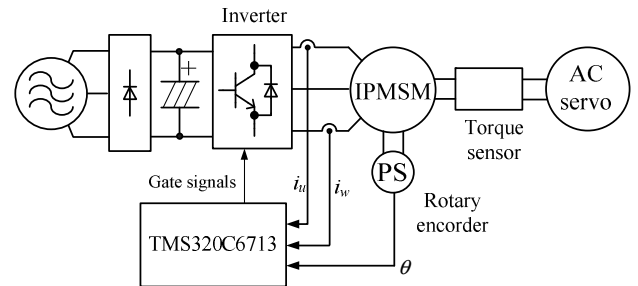
Fig. 2. Experimental system.
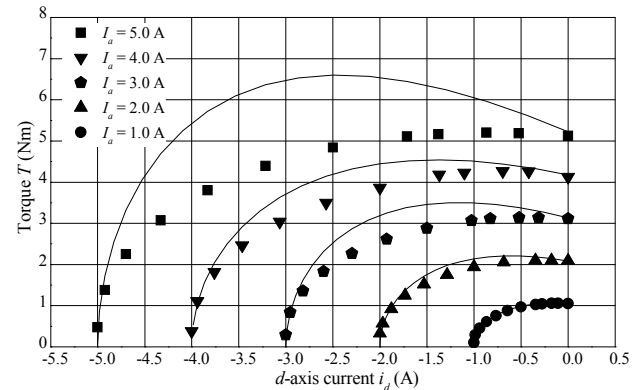
Fig. 3. Torque characteristic.
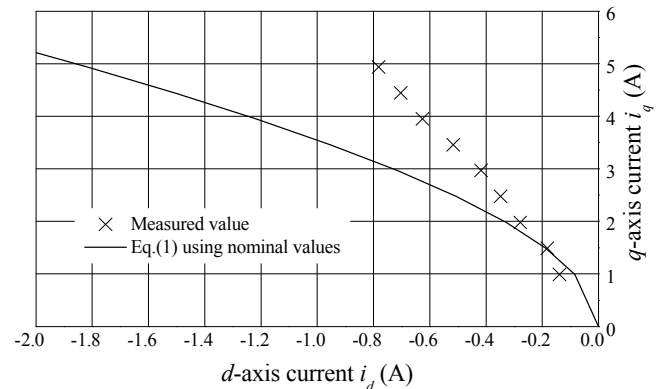
Fig. 4. Maximum torque per ampere control curves.

error between the true and the calculated MTPA curves is notably enlarged as the magnetic saturation becomes remarkable. As mentioned above, the MTPA control is detrimentally affected by the magnetic saturation. Therefore,

the operating points must be correctly modified according to the operating situation.

IV. PROPOSED IDENTIFICATION STRATEGY

The parameter identification method have been proposed[7]-[11]. In this paper, the strategy using the instantaneous reactive power is focused on. The instantaneous reactive power Q is calculated by a vector product of the two phase currents and voltages on the stator reference frame and the synchronously rotating reference frame as

$$Q = \frac{3}{2} \begin{bmatrix} i_\alpha \\ i_\beta \end{bmatrix} \times \begin{bmatrix} v_\alpha \\ v_\beta \end{bmatrix} = \frac{3}{2}(i_\alpha v_\beta - i_\beta v_\alpha)$$
$$= \frac{3}{2} \begin{bmatrix} i_d \\ i_q \end{bmatrix} \times \begin{bmatrix} v_d \\ v_q \end{bmatrix} = \frac{3}{2}(i_d v_q - i_q v_d) \tag{4}$$

Then the command voltages in the controller are used for v_d and v_q. The voltage equation of the IPM motor in the steady state is given by (5). The instantaneous reactive power is also obtained as (6) by substituting (5) into (4);

$$\begin{bmatrix} v_d \\ v_q \end{bmatrix} = \begin{bmatrix} R_a & -\omega L_q \\ \omega L_d & R_a \end{bmatrix} \begin{bmatrix} i_d \\ i_q \end{bmatrix} + \begin{bmatrix} 0 \\ \omega \psi_f \end{bmatrix}, \text{ and} \tag{5}$$

$$Q = \frac{3}{2}\omega(L_d i_d{}^2 + L_q i_q{}^2 + \psi_f i_d) . \tag{6}$$

According to (4) and (6), the armature winding resistance R_a is not included at all in both equations. Therefore, the instantaneous reactive power is never affected by the variation of R_a caused by the temperature change[12].

In order to identify L_d and Ψ_f, the high-frequency signal whose angular frequency is ω_h and amplitude is i_{dh} is injected to the d-axis current control loop. This can be achieved by superimposing the high-frequency current command onto the d-axis current command. In the case, (6) is rewritten as follows:

$$Q = \frac{3}{2}\omega\{(L_d i_d{}^2 + L_q i_q{}^2 + \psi_f i_d) + \frac{L_d}{2} i_{dh}{}^2$$
$$+ (2L_d i_d + \psi_f)i_{dh}\cos\omega_h t + \frac{L_d}{2}i_{dh}{}^2\cos 2\omega_h t\}. \tag{7}$$

As shown in (7), Q has a ω_h component and a $2\omega_h$ component as well as the DC component. If ω_h component is separated from other components with a band-pass filter (BPF), the third term that does not include L_q can be extracted. It is preferable to set i_{dh} as small as possible. Therefore, the forth term is very small, and this means that it is impossible to use the $2\omega_h$ component for the d-axis inductance identification. In addition, the mathematical model $\hat{Q}_\psi$ which has only the information of $\hat{\psi}_f$ is obtained as (8) if the d-axis current is controlled to be zero;

$$\hat{Q}_\psi = \frac{3}{2}\omega\hat{\psi}_f i_{dh}\cos\omega_h t . \tag{8}$$
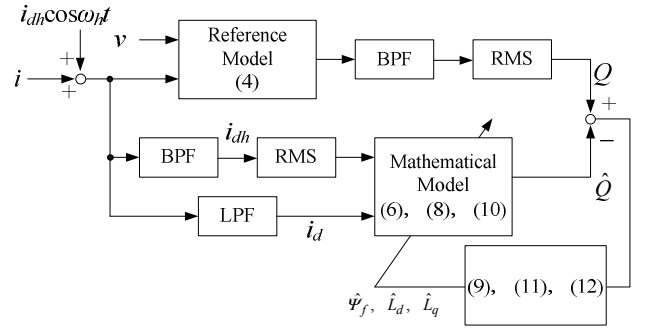
Fig. 5. Identification system.

As shown in the identification system depicted in Fig. 5, the mathematical model (8) and the magnetic flux linkage are dynamically modified on the basis of the following identification algorithm:

$$\hat{\psi}_f = \gamma_\psi \int \frac{Q_\psi - \hat{Q}_\psi}{\omega i_{dh}\cos\omega_h t} dt , \tag{9}$$

where γ_ψ is the identification gain. $\hat{\psi}_f$ is updated until the error between the reference model and the mathematical model converges to zero.

After the above identification process completes, the mismatch of ψ_f in the third term of (7) becomes zero. The mathematical model $\hat{Q}_{Ld}$ is given by

$$\hat{Q}_{Ld} = \frac{3}{2}\omega(2\hat{L}_d i_d + \psi_f)i_{dh}\cos\omega_h t . \tag{10}$$

L_d can be identified by using the following algorithm in the similar manner:

$$\hat{L}_d = \gamma_{Ld} \int \frac{Q_{Ld} - \hat{Q}_{Ld}}{2\omega i_d i_{dh}\cos\omega_h t} dt , \tag{11}$$

where Q_{Ld} is the reference model and γ_{Ld} is the identification gain.

Similarly to the case of ψ_f, $\hat{L}_d$ converges to the true value by integrating the error between the reference model and the mathematical model. The denominator of (9) and (11) has multiple zero cross points because it includes $\cos\omega_h t$. In order to avoid the division by the zero, the parameter identification is carried out by using the root mean squared value as shown in Fig. 5.

Since the mismatch of L_d and ψ_f have been canceled out by the above technique, L_q can be identified by using the DC component of (6) which is filtered out of (7) by using the LPF. The modified equation is given by

$$\hat{L}_q = \gamma_{Lq} \int \frac{Q - \hat{Q}}{\omega i_q{}^2} dt , \tag{12}$$

where Q is the reference model, $\hat{Q}$ is the mathematical model and γ_{Lq} is the identification gain. According to the above

795
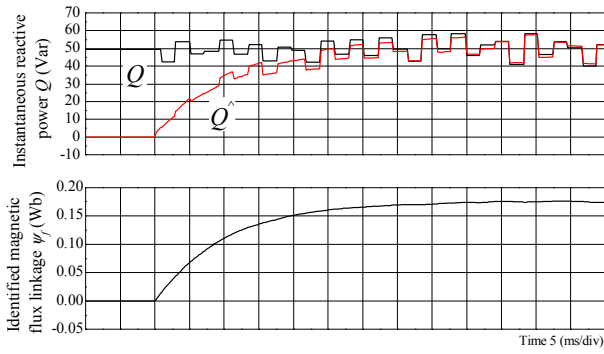
Fig. 6. Magnetic flux linkage identification characteristic.
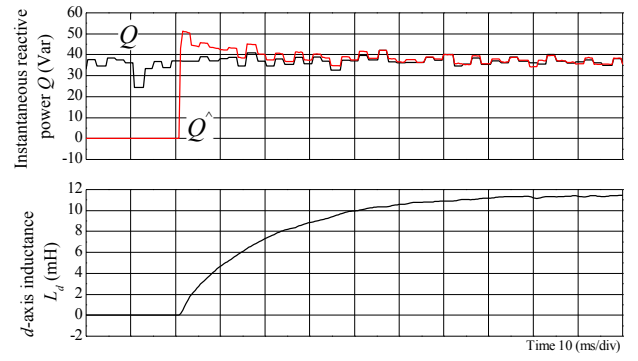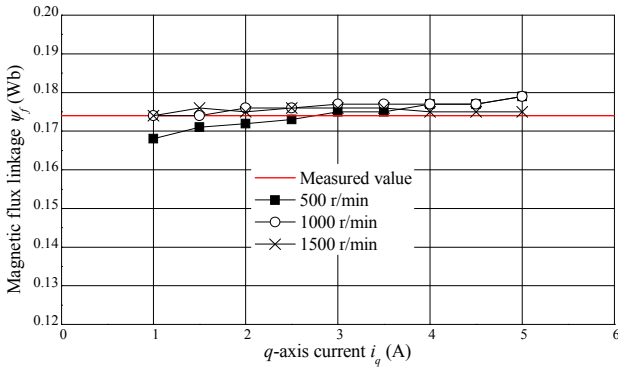
Fig. 7. Experimental results of magnetic flux linkage identification.

Fig. 8. d-axis inductance identification characteristic.
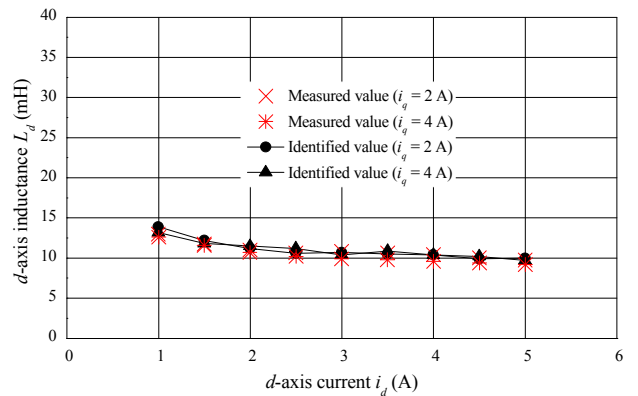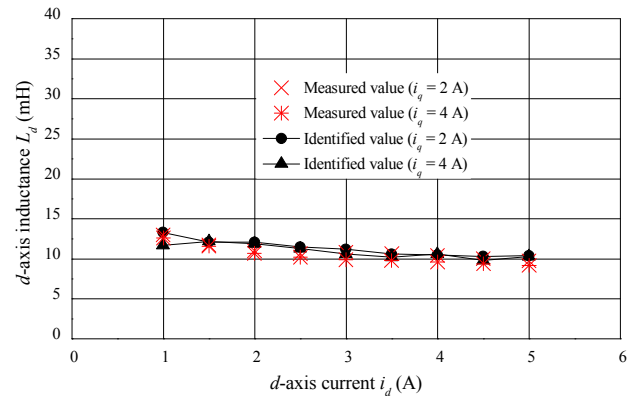
(a) 500 r/min

(b) 1500 r/min

Fig. 9. Experimental results of d-axis inductance identification.

technique, each parameter can be identified independently by the high-frequency signal superimposed onto the d-axis current command. Additionally, the identification time becomes constant regardless of the rotating speed by setting the identification gain as an inverse function of the injected frequency[13]-[15]. The MTPA curve is corrected by the parameters identified by the method described above. Assuming that the proposed method is applied for the motor mounted on the vehicle, the filter time constant of the current commands is very large, i.e, the LPF with an approximately 500-ms time constant is inserted in the current control system; thus, the current varies slowly. Therefore, the proposed identification strategy must identify parameters in less than 500 ms.

V. EXPERIMENTAL RESULTS

A. Magnetic Flux Linkage Identification

Figure 6 shows the dynamic identification characteristic of the magnetic flux linkage based on (9) at 1000 r/min. The current command is set to the following values: i_d^*=0 A and i_q^*=3 A. In (8), the high frequency signal condition is set to the following values: i_{dh}=0.3 A and ω_h=2000π rad/s. Figure 7 shows the experimental result of the magnetic flux linkage identification when the rotating speed is controlled at the constant value and the q-axis current is varied.

As shown in Fig. 6, the mathematical model stably converges to the reference model. It was confirmed that the identified value of the magnetic flux linkage converges to the true value in the test, where the identification time is 50 ms. The identification is completed within 1/10 of the time constant of the current command. In Fig. 7, the solid line shows the measured values of the magnetic flux linkage which is 0.174 Wb. It can be seen that the proposed method can identify the magnetic flux linkage within 5 % error regardless of the rotating speed and the q-axis current.
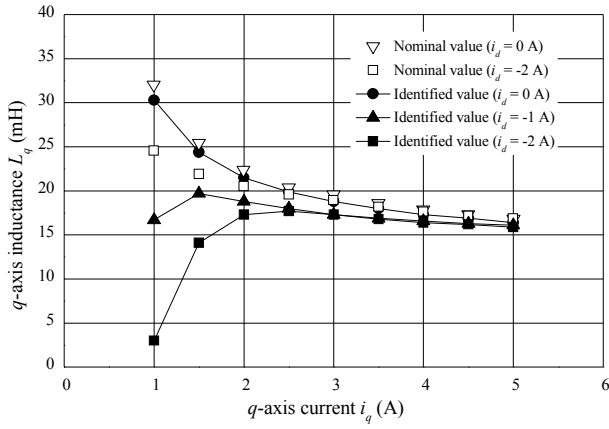
(a) 500 r/min
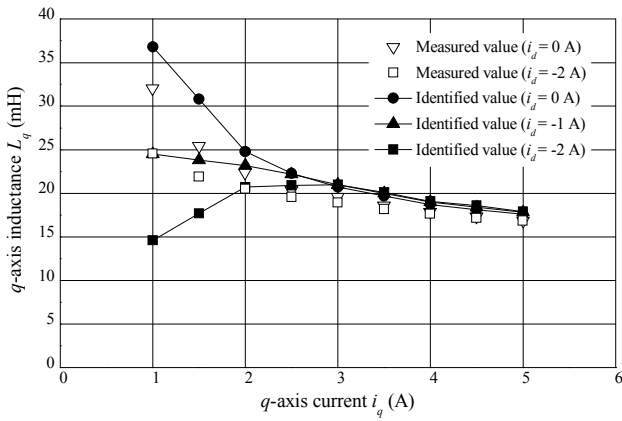
(b) 1500 r/min

Fig. 10. Experimental results of *q*-axis inductance identification.

B. *d*-Axis Inductance Identification

The *d*-axis inductance identification is carried out after the mismatch of the magnetic flux linkage has been eliminated. Figure 8 shows the dynamic convergence characteristic of the *d*-axis inductance identification which is based on (11). The rotating speed is 1000 r/min, and the current commands are set at i_d=-3A and i_q=3A. The injected high-frequency signal is the same as the case of the magnetic flux linkage identification. The experimental results of the *d*-axis inductance at 500 r/min and 1500 r/min are shown in Figs. 9 (a) and 9(b). The *d*-axis inductance saturation characteristic is also depicted in Fig.9.

The convergence time is 70 ms as demonstrated in Fig. 8. In comparison of the identified and the measured saturation characteristics, the figure shows very good agreement between them regardless of the rotating speed and the current amplitude.

C. *q*-Axis Inductance Identification

The *q*-axis inductance is identified after the above mentioned identification processes, which is in the case of no-parameter mismatches in the magnetic flux linkage and the *d*-axis inductance. Figures 10 (a) and 10(b) show the
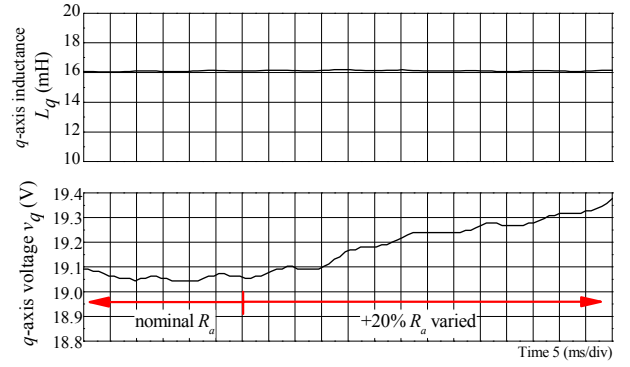
Fig. 11. Impact of winding resestance variation on *q*-axis inductance identification characteristic.
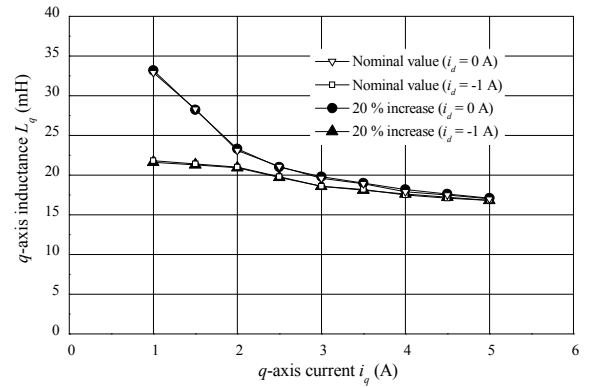
Fig. 12. Parameter sensitivity of winding resistance to *q*-axis inductance identification.
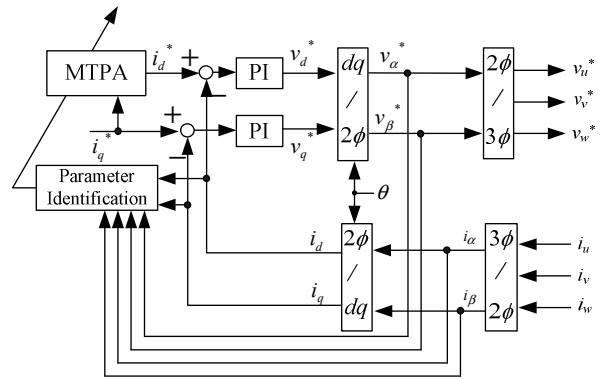
Fig. 13. Adaptive MTPA control system.

experimental results based on (12) and the measured saturation characteristics of the *q*-axis inductance at 500 r/min and 1500 r/min, respectively. Although the error between the identified and the measured values is observed in the low *q*-axis current range, the both characteristics agree very well as the *q*-axis current increases. The reason of the error is the minute mismatch of the magnetic flux linkage and the *d*-axis inductance. The *q*-axis inductance identification algorithm (12) is discussed on the assumption of no mismatches of the magnetic flux linkage and the *d*-axis inductance, but from Figs. 7 and 9, the small identification error is observed. Therefore, in the low instantaneous reactive power range, the

impact of these errors is large enough to affect detrimentally the *q*-axis inductance identification.

D. *Verification of Parameter Sensitivity*

In order to verify the impact of the armature resistance variation caused by the temperature rise, the resisters are intentionally inserted between the inverter and the IPMSM. Assuming the situation where the armature resistance varies by +20 % of the nominal value, the inserted resistance value is 0.2 Ω. Figure 11 shows the *q*-axis inductance identification characteristics when the external resistance is inserted. The current command is set at i_d=0 A and i_q=5 A. The comparison of the *q*-axis saturation characteristics is shown in Fig. 12. The rotating speed is 1000 r/min, and the *d*-axis current is controlled to be constant; i_d=0 A and i_d=-1 A in the test.

As shown in Fig.11, even if the armature resistance increases by 20 %, the identified parameter is not affected by the resistance variation at all. The identification characteristics when the external resistance is inserted agree with those of the nominal value as shown in Fig.12. This experimental result verifies that the proposed method has no sensitivity to the armature resistance.

E. *Adaptive Modification of MTPA Curve*

The MTPA curve given by (1) is modified by the parameters identified by the above mentioned technique as shown in Fig. 13. Figure 14 shows the three MTPA curves, i.e., the MTPA curve calculated by (1) using the nominal parameters, the MTPA curve sought by the experimental measurement and the MTPA curve recalculated by (1) using the identified parameters by the proposed technique. In Fig. 14, the measured value is identical to the plots in Fig. 4, and the plots of the nominal values are obtained by substituting the nominal parameters to (1). The plots of the identified values are also given by modifying (1) by using the identified parameters. Figures 15 (a) and 15(b) show the MTPA characteristics at 500 r/min and 1500 r/min. These are calculated by dividing the motor torque by the current amplitude. Similarly to Fig. 14, the measured values (the true MTPA curve), the calculated values by substituting the nominal values into (1), and the modified MTPA values by using identified parameters are plotted.

As can be seen in Fig. 14, the MTPA control points using the nominal values digress from the optimum points. The MTPA curve is turned to watch the measured curve (the true MTPA curve). The motor torque per unit current amplitude is improved by using the proposed method as shown in Fig. 15. Particularly the effectiveness of the proposed method is remarkable as the *q*-axis current increases. The MTPA characteristic agrees well with the measured characteristic regardless of the rotating speed. It is found that the test motor can be controlled to deliver the maximum torque per unit current amplitude by applying the proposed method.

VI. Conclusion

In this paper, a robust MTPA control strategy against the motor parameter variations caused by the magnetic saturation and the temperature change has been proposed. It has been
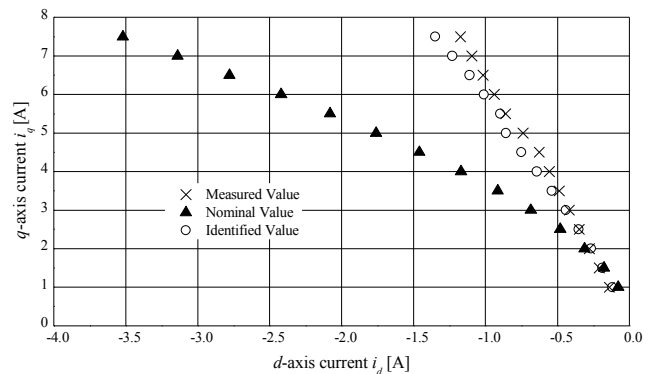
Fig. 14. Comparison of MTPA curves.
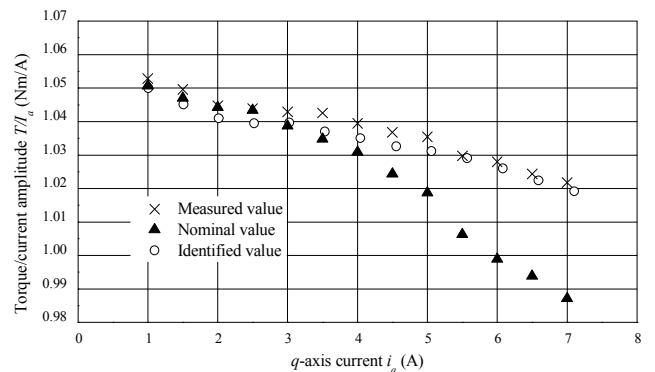
(a) 500 r/min
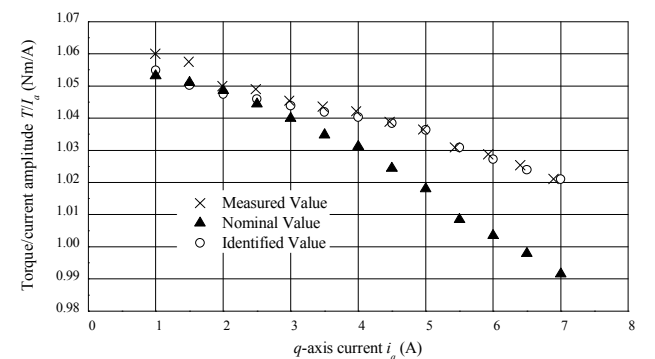
(b) 1500 r/min

Fig. 15. Comparison of MTPA characteristics.

confirmed that the proposed method can identify the magnetic flux linkage, the *d*-axis inductance and the *q*-axis inductance by using the instantaneous reactive power which has no sensitivity to the armature winding resistance. The identification time of these parameters are within 500 ms, and the identification errors are within 5 %. It is substantiated that the proposed method is not affected to the temperature variation. The deviated operating points which are calculated by the MTPA formulas can be properly modified by using the identified parameters; hence, the motor is always controlled to track on the true MTPA curve. It was confirmed that the motor torque per unit current norm can be maximized.

REFERRENCE

[1] Lei Ma, M. Sanada, S. Morimoto and Y. Takada: "Extended Operating Range and High Efficiency Adjustable Speed Control of IPMSM with Variable PM Armature Flux Linkage", *IEEE Trans.*, Vol. 120, No. 8-9, pp. 1031-1036 (2000)

[2] G.Pellegrino, A.Vagati, B.Boazzo and P.Guglielmi: "Comparison of Induction and PM Synchronous Motor Drives for EV Application Including Design Examples", *IEEE Trans.*, Vol. 48, No. 6, pp. 2322-2332 (2012)

[3] T. M. Jahns, G.B. Kliman and W. Thomas: "Interior Permanent-Magnet Synchronous Motors for Adjustable-Speed Drives", *IEEE Trans. on Ind. Appl.*, vol. IA-22, No.4, pp.738-747 (1986)

[4] Quoc Khanh Nguyen, Matthias Petrich and Jorg Roth-Stielow: "Implementation of the MTPA and MTPV control with online parameter identification for a high speed IPMSM used as traction drive", The 2014 International Power Electronics Conference, 19P4-2(2014)

[5] G. Stumberger, B. Stumberger, and D. Dolinar: "Evaluation of saturation and cross magnetization effects in interior permanent magnet synchronous machine", *IEEE Trans. Ind. Appl.*, Vol. 39, No.5, pp.1264-1271 (2003)

[6] S. Lerdudomsak, S. Doki and S. Okuma: "Method to Calculate Reference Currents to Achieve Fast Torque Response of IPMSM": *IEEJ Trans.*, Vol. 131, No. 1, pp. 45-52 (2011)

[7] S. J. Underwood and I. Husain: "Online Parameter Estimation and Adaptive Control of Permanent-Magnet Synchronous Machines", *IEEE Trans. Ind. Electron.*, Vol. 57, No. 7, pp.2435-2443 (2010)

[8] T. L. Vandoorn , F. M. De Belie , T. J. Vyncke , J. A. Melkebeek and P. Lataire: "Generation of multisinusoidal test signals for the identification of synchronous-machine parameters by using a voltage-source inverter", *IEEE Trans. Ind. Electron.*, Vol. 57, No. 1, pp.430-439 (2010)

[9] P. Niazi and H. A. Toliyat: "Online Parameter Estimation of Permanent-Magnet Assisted Synchronous Reluctance Motor", *IEEE Trans. on Ind. Appl.*, vol. 43, No.2, pp.609-615 (2007)

[10] S. Kallio, J. Karttunen, P. Peltoniemi, P. Silventoinen and O. Pyrhonen: "Online Estimation of Double-star IPM Machine Parameters Using RLS Algorithm", *IEEE Trans. Ind. Electron.*, Vol. 61, No. 9, pp.4519-4530 (2014)

[11] T. Marcic, B. Stumberger and G. Stumberger: "Differential-Evolution-Based Parameter Identification of a Line-Start IPM Synchronous Motor", *IEEE Trans. Ind. Electron.*, Vol. 61, No. 11, pp.5921-5929 (2014)

[12] T. Noguchi, K. Yamada, S. Kondo and I. Takahashi: "Quick-Response Torque Control of Induction Motor with Robustness against Variations of Primary and Secondary Resistances", *IEEJ Trans.*, Vol. 115-D, No. 9, pp. 1115-1122, (1995)

[13] M. Ohara and T. Noguchi: "Performance Improvement of Rotor Position Estimator for Sensorless Control of Permanent Magnet Motor Based on Model Reference Adaptive System", *IEEJ Trans. Ind. Appl.*, Vol. 133, No. 2, pp. 222-230 (2013)

[14] T. Orlowska-Kowalska and M. Dybkowski: "Stator-Current-Based MRAS Estimator for a Wide Range Speed-Sensorless Induction-Motor Drive", *IEEE Trans. Ind. Electron.*, Vol. 57, No. 4, pp.1296-1308 (2010)

[15] R. Pena, R. Cardenas, J. Proboste, G. Asher and J. Clare: "Sensorless Control of Doubly-Fed Induction Generators Using a Rotor-Current-Based MRAS Observer", *IEEE Trans. Ind. Electron.*, Vol. 55, No. 1, pp.330-339 (2008)